Halogen, Chalcogen, and Pnicogen Bonding involving Hypervalent Atoms

Steve Scheiner* and Jia Lu
Department of Chemistry and Biochemistry
Utah State University
Logan, UT 84322-0300

*email: steve.scheiner@usu.edu
phone: 435-797-7419

ABSTRACT

The additional substituents arising from hypervalency present a number of complicating issues for the formation of noncovalent bonds. The XF_5 molecule (X=Cl, Br, I) was allowed to form a halogen bond with NH_3 as base. Hypervalent chalcogen bonding is examined by way of YF_4 and YF_6 (Y=S, Se, Te), and ZF_5 (Z=P, As, Sb) is used to model pnicogen bonding. Pnicogen bonds are particularly strong, with interaction energies approaching 50 kcal/mol, and also involve wholesale rearrangement from trigonal bipyramidal in the monomer to square pyramidal in the complex, subject to a large deformation energy. YF_4 chalcogen bonding is also strong, and like pnicogen bonding, is enhanced by a heavier central atom. XF_5 halogen bond energies are roughly 9 kcal/mol, and display a unique sensitivity to the identity of the X atom. The crowded octahedral structure of YF_6 permits only very weak interactions. As the F atoms of SeF_6 are replaced progressively by H, a chalcogen bond appears in combination with $SeH\cdot\cdot N$ and $NH\cdot\cdot F$ H-bonds. The strongest such chalcogen bond appears in $SeF_3H_3\cdot\cdot NH_3$, with a binding energy of 7 kcal/mol, wherein the base is located in the H_3 face of the Lewis acid. Results are discussed in the context of the way in which the positions and intensities of σ-holes are influenced by the locations of substituents and lone electron pairs.

1. INTRODUCTION

After many decades of intense study, the hydrogen bond (HB) has rewarded researchers [1-4] with a rich trove of interesting and useful insights into its nature. Although assumed for many years to be a unique sort of interaction, more recent work has demonstrated that the HB has a number of noncovalent bonding sisters [5-21]. The replacement of the bridging proton by any of a host of electronegative atoms from the right side of the periodic table yields an attractive force with many parallels to the HB. This group of bonds usually assume the name of the family of the bridging atom, whether halogen, chalcogen, pnicogen, or tetrel, and share many features with one another. For example, the HB is held together in part by a Coulombic attraction between the partially positive bridging H and a partial negative charge on the proton acceptor atom. The same is true of its cousins, but with a small wrinkle. While the proton contains a positive charge, the more electronegative atoms are characterized by an overall negative charge. However, this charge is not uniformly distributed. Indeed, the potential surrounding the halogen atom X of an R-X bond has a positive pole directly opposite the R group, which is surrounded by a negative equator. This positive region is commonly referred to [22] as a σ-hole, and attracts the negative charge of an approaching nucleophile. Just as in the case of the HB, the bonding within this halogen bond (XB) is not purely electrostatic, but is supplemented by attractions due to electronic redistributions, under various rubrics such as charge transfer, polarization, orbital mixing, induction, etc. To all this is added a dispersive attractive force.

The same sort of reasoning that pertains to HBs and XBs applies to other noncovalent bonds with some minor differences. Unlike the single σ-hole associated with the halogen atom, other atoms, e.g. chalcogen or pnicogen, are typically surrounded by more than one σ-hole. In general, there is one such positive region associated with each covalent bond in which the atom in question participates. The nucleophilic base that participates in each such interaction tends to approach the Lewis acid along the direction of a σ-hole so as to maximize the Coulombic attraction. Another factor that controls the mutual orientation of the two groups involves orbital overlap. The same R-X σ-bond that is the source of the depletion of electron density in the σ-hole has associated with it a σ* antibonding orbital that has its maximum amplitude in the same location as the σ-hole. It is into this σ* antibonding orbital that the base (B) transfers some of its charge, so the charge transfer is likewise amplified by the maximum overlap of the nucleophile's lone pair with this orbital, which is in turn maximized by a linear R-X···B arrangement.

For the same reason that a nucleophile is attracted toward a σ-hole and its associated σ* antibonding orbital, it would be repelled away from a lone pair on the X atom and its attendant partial negative charge. This repulsion would generally amplify the push of the base toward a σ-hole, as the latter tends to appear in between the lone pairs. In the halogen bond, for example, the three X lone pairs surround the R-X axis, and would thus reinforce the inclination of a nucleophile toward this axis and linearity. The single lone pair of the pnicogen Z

atom of ZR_3 likewise occurs well off any of the three Z-R axes. Taking the ideal case of tetrahedral arrangement of the Z lone pair and the three Z-R bonds, the lone pair would be located 69.5° from each σ-hole.

While halogen, chalcogen, and pnicogen atoms typically participate respectively in one, two, and three covalent bonds, they are also quite prone to hypervalent bonding situations which involve a larger number of covalent bonds. The geometrical issues become more complicated, and cramped, when such hypervalency occurs. In the first place, a large number of substituents surrounding the central atom would present steric obstructions and a more limited path to the approach of an incoming base. There are also factors arising from positioning of bonds and lone pairs. Taking as an example the case of a central halogen in a XR_5 pentavalent bonding situation, the five X-R bonds combine with the single X lone pair to yield an overall octahedral structure, with the five X-R bonds occupying the vertices of a square pyramid. The four X-R bonds in the base of the pyramid lie directly opposite one another, precluding the appearance of a σ-hole opposite any of these bonds. The position opposite the apical X-R bond is occupied by the X lone pair, again preventing the appearance of a σ-hole and impeding the approach of a nucleophile. So in the absence of other factors, one would expect that a XR_5 molecule could not participate in a XB. Yet there have in fact been observations [23-26] of halogen bonding in such systems, so there are obviously other issues that must be considered. The current work is dedicated to an improved understanding of the way in which hypervalency affects the ability of halogen, as well as chalcogen, and pnicogen atoms to participate in noncovalent bonds.

The issue of the interplay between noncovalent bonding and hypervalency has seen only limited prior study in the literature. Of the various sorts of interactions, much of the previous work concerned halogen bonds (XBs) [23-27]. Moreover the bulk of the studies have been further limited to trivalent halogen atoms which would not present steric crowding as an important effect. Even when the valency is extended to five, as in the case of XF_5, its square pyramidal shape allows a path of a base to the central X atom that is not obstructed by the surrounding substituents. In the case of a hypervalent chalcogen atom, the see-saw shape of SF_4 likewise presents little in the way of a steric obstacle to formation of a S··N chalcogen bond [28], nor is this a problem in a YO_2X_2 bonding situation [29] with Y a chalcogen atom, nor for SO_3 [30]. There has been some study of hypervalent pnicogens (Z), specifically in the case of four substituents as in ZOF_2X, ZOF_3, and ZH_2FO [31, 32] but little was described concerning any geometrical changes in the monomer required to accommodate the base, nor the energetic consequence of any such distortion. Crystal studies [33] have suggested that a pentavalent ZF_5 molecule normally in a trigonal bipyramid shape undergoes a major rearrangement, molding itself into a square pyramidal arrangement upon formation of a pnicogen bond, but again left unresolved the question of the energetic consequence of such a rearrangement. In the related case of aerogen bonding to a central noble gas atom, a hexavalent or other hypervalent bonding situation clearly obstructs the path of a base, but not to the

point where a noncovalent bond is unable to form [34-37], even though a hexavalent arrangement of substituents around any central atom precludes the presence of a σ-hole opposite any of these covalent bonds.

The issue of steric crowding in hypervalent situations thus appears to represent a ripe area for study in the context of noncovalent bonds. To the issue of steric repulsions between the base and the substituents must be added consideration of any lone pairs which will not only tend to repel the base, but also affect the position and intensity of any σ-holes that would serve to pull the base in toward the central atom. This work thus addresses these issues in a systematic manner. Hypervalent halogen, chalcogen, and pnicogen atoms were considered as central atoms and their ability to engage in interactions with an incoming base are examined. The influence of any lone pairs on the central atom upon the positioning and intensity of the σ-holes is elucidated, as well as the way in which the σ-hole locations in turn affect the geometry and energetics of the ensuing complex. Due to a number of steric interactions, there is a certain degree of geometrical deformation within the monomers that occur as the Lewis acid and base approach one another. The particular distortions, and their energetic consequence upon the noncovalent bond, are studied in some detail.

2. SYSTEMS AND METHODS

Pentavalent halogens of the type XF_5 were considered for central halogen atoms X=Cl, Br, and I. Both tetra- and hexavalent chalcogens were examined via YF_4 and YF_6, where S, Se, and Te were considered for Y. The normal trivalency of pnicogens was extended to ZF_5 for Z=P, As and Sb. In addition to the perfluorinated molecules with their very electron-withdrawing substituents, it is necessary to evaluate how the results might differ with less electronegative groups. For this purpose, the chalcogen-bonding SeF_6 was taken as a sample system, and the six F atoms replaced one by one by H. For a number of the resulting SeF_nH_{6-n} molecules, there are more than one isomer possible, so each was studied individually in order to achieve a full and comprehensive picture. Each of the Lewis acid molecules was paired with NH_3 as prototype base, to take advantage of several of its virtues. In the first place, NH_3 serves as a simple model of amines which are common bases in these interactions. The single N lone pair nucleophilic site avoids complications that would otherwise arise in terms of competition for the electrophilic sites on the acid. The small size of the molecule further avoids interactions secondary to the noncovalent bonds of interest. Lastly, the weak acidity of NH_3's protons minimize the stability of HBs that would draw the dimer configuration away from the noncovalent bonds of interest. All told, 25 different dimer structures were considered, in addition to a number of plausible equilibrium geometries which proved on detailed searching to not represent true minima on the potential energy surface.

Quantum calculations were executed at the MP2 level using the Gaussian-09 [38] program suite. The aug-cc-pVDZ basis set was applied to all atoms with the exception of fourth-row atoms I, Te, and Sb, which were represented by the aug-cc-pVDZ-PP pseudopotential [39, 40] which takes relativistic effects into account. The

accuracy and effectiveness of this level of theory has been demonstrated in numerous previous studies [41-49] of related systems.   All geometries were fully optimized, and checked by frequency calculations to ensure they were true minima. The binding energy, E_b, is defined as the energy difference between the complex on one hand, and the sum of the energies of the optimized monomers, and was corrected for basis set superposition error via the counterpoise procedure [15, 50, 51]. The interaction energy E_{int} of each dimer differs in that it involves the energies of the monomers within the context of their geometry within the dimer. As such, this quantity represents the interaction between two monomers that have already been deformed into the structures they will ultimately adopt within the dimer. Thus, the binding and interaction energies differ by the distortion energy of each monomer that takes it from its optimized structure to that within the dimer. Molecular electrostatic potentials surrounding each molecule were analyzed by the Multiwfn program [52] to locate its maxima and minima on the isodensity surface corresponding to $\rho=0.001$ au. Charge transfer was evaluated by the Natural Bond Orbital (NBO) technique [53]. The AIM formalism elucidated bond paths via analysis of the topology of the electron density [54, 55], making use of the AIMALL program [56]. Decomposition of the total interaction energy was accomplished using the symmetry-adapted perturbation theory (SAPT) approach [57, 58], with the aid of the MOLPRO program [59].

3. RESULTS

3.1 Perfluorinated Lewis Acids

The optimized geometries of the complexes of the various perfluorinated molecules with NH_3 are displayed in Fig 1 which clearly shows the different sorts of structures. The XF_5 monomers with their lone pair on the central atom adopt a square pyramidal shape which persists in the complex. So there is a competition of sorts in terms of the preferred site for an approaching nucleophile. On one hand the lone pair that sits opposite the apical F atom would tend to repel the nucleophile. But a position opposite the apical X-F bond would have a tendency for a positive region of the MEP as the electronegative F atom sucks electron density out of this area, in a so-called σ-hole. In the case of IF_5, the lone pair predominates, and the σ-hole appears 135º from the F-I axis, a distortion of 45º from where it would be located in the absence of the I lone pair. It is for this reason that the NH_3 is also removed from a position directly opposite the apical F, with a θ(FI··N) angle of 145º. This same deviation of the MEP maximum from linearity appears also in ClF_5 and BrF_5, and in almost the same amount, with respective angles of 147° and 142° respectively. It is therefore interesting to see in Fig 1 that the effect of this displacement of the σ-hole has no effect on ClF_5··NH_3 where the N is precisely opposite the apical F. (More on this system below.) There is more of an influence for the Br analogue but the 168° (F-Br··N) angle is still much closer to linearity than would be indicated by the σ-hole. Perhaps the growing influence of the σ-hole position with larger X atom reflects the larger magnitude of $V_{s,max}$, which is collected in the last column of Table 1.

As the central halogen atom grows in size one sees that the intermolecular $R(X \cdot \cdot N)$ distance elongates quite significantly from 2.07 to 2.91 Å. As may be seen in Table 1, the shortness of the $R(Cl \cdot \cdot N)$ distance is reflected in a much stronger binding energy than for the other two halogen atoms. The density at the $X \cdot \cdot N$ bond critical point is likewise much larger for Cl, as are the NBO measures of halogen bond strength. E(2) in Table 1 refers to the transfer from the N lone pair to the $\sigma^*(X-F)$ antibonding orbital of the apical F atom. There is also some transfer into the other $\sigma^*(X-F)$ orbitals of the other F atoms, denoted E(2)* in Table 1. In the case of ClF_5, the former is quite large, and the latter only amounts to a total of 0.99 kcal/mol for the two secondary interactions. But the situation is quite different for X=Br and I, where the total secondary transfers are cumulatively larger than that involving the apical F. Nonetheless, by all measures the $Cl \cdot \cdot N$ halogen bond is quite a bit stronger than that for the two heavier halogens. This trend is opposite to that which would have been predicted based upon the intensity of the σ-hole, listed as $V_{s,max}$, evaluated at $\rho=0.001$ au, in the penultimate column of Table 1. This quantity increases in the order Cl < Br < I, which fulfills expectations based upon electronegativity and polarizability. But its behavior contrary to halogen bond strength demonstrates that this aspect of the MEP is a poor indicator.

Part of the explanation of this deviation arises because the $Cl \cdot \cdot N$ bond has some of the hallmarks of a covalent bond, at least in part. Its bond length of 2.067 Å is only slightly longer than the F-Cl bonds which all exceed 1.8 Å. The large density at its bond critical point of 0.11 au approaches that of true covalent bonds, only 0.03 au smaller than the same quantities for the Cl-F bonds. The formation of this bond also induces a good deal of distortion of the ClF_5 monomer. There is a very large 30 kcal/mol difference between the binding and interaction energies in this complex which is due to the monomer deformation energy which stretches the Cl-F bonds by more than 0.1 Å upon forming the complex with NH_3. The incipient Cl-N bond also causes the four F atoms in the pyramid base to move outward, away from the apical F, by 9°. This sort of motion toward the Cl-N bond would be consistent with a picture wherein the bulky Cl lone pair is pulled and constricted as it engages in a covalent bond with N, thereby reducing its repulsions with the four Cl-F bonds. None of the above are true of the complexes of NH_3 with BrF_5 and IF_5, which retain their noncovalent halogen bond character.

Turning next to chalcogen atoms Y, one can envision either a hexavalent or tetravalent bonding situation. The YF_6 atoms will have no Y lone pairs while there will be one such pair in YF_4. The YF_6 molecule will take on an octahedral shape so be unable to develop a σ-hole directly opposite any F atom. Instead, each such hole appears on a face of the octahedron, equally spaced between three F atoms. It is therefore to this point which a nucleophile is attracted, as illustrated in Fig 1. But partly due to the congested nature of this area, coupled with the fairly small values of $V_{s,max}$, less than 40 kcal/mol, the N is unable to approach the Y atom very closely, with $R(Y \cdot \cdot N)$ distances all close to 4 Å. The shortest distance is associated with Y=Te. Indeed it is only for this large Y atom that there is any evidence of a chalcogen bond at all. Both SF_6 and SeF_6 are bonded to NH_3 via a

pair of NH··F H-bonds, as indicated by both AIM and NBO. While AIM does not register a true chalcogen bond for TeF_6, there is some NBO evidence. While there is no single Te-F bond directly opposite the N, there are three such bonds, which are partially opposite. The cumulative E(2) for transfer into these three σ*(Te-F) antibonds sums to 0.33 kcal/mol, and NBO shows no indication of a NH··F HB. The transition from H-bonds to a chalcogen bond on going from Se to Te is aided by the intensification of $V_{s,max}$ which rises to 38 kcal/mol for the larger atom. But in any case, the interaction between NH_3 and the hexafluorinated chalcogens, whether H-bond or chalcogen bond, is very weak, never exceeding 1 kcal/mol. Note, however, that if three of the F atoms of TeF_6 are replaced by H, the situation changes. The σ-hole on the H_3 face of the TeF_3H_3 molecule doubles in magnitude, and the N is pulled in to R(Te··N)=3.165 Å. The binding energy climbs up to 7.6 kcal/mol, and both NBO and AIM verify the presence of a true chalcogen bond, with only minimal H-bond contribution. It is worth stressing that the NH_3 approaches the Te directly, forgoing the possibility of an approach along a TeH bond axis which could potentially result in a strong and linear TeH··N H-bond.

The alteration from hexavalent to tetravalent chalcogen produces a YF_4 monomer which contains a Y lone pair. The monomer thus adopts a "see-saw" geometry which includes a pair of axial F atoms, and two of the three equatorial sites are occupied by F atoms. There are thus openings in the equatorial plane where a nucleophile might approach Y. At the same time the NH_3 needs to avoid the Y lone pair which also lies in the equatorial plane. The σ-holes for YF_4 do indeed avoid the Y lone pair, lying 13º from a position directly opposite each of the equatorial F atoms. It is this avoidance of the lone pair that causes the F-Y··N angles in Fig 1 to all be somewhat less than 180º. This deviation from F-Y··N linearity is smallest for SF_4 and increases as the chalcogen atom is enlarged. The intermolecular distance is at a maximum for Y=S, diminishes for Se, and then increases a small amount for Te. Some of the other measures of the chalcogen bond strength also reflect this trend with E(2) and ρ_{BCP} at their maxima for Se. On the other hand, the quickly rising values of E(2)* suggest that the secondary transfers into the three other Y-F antibonding orbitals are partly responsible for the similarly precipitous S < Se < Te increase in binding energy from 6.6 to 16.0 kcal/mol. It might be noted that a similar order pertains to $V_{s,max}$, evaluated at ρ=0.001 au. The difference between E_b and E_{int} reflects the deformation energy that occurs as the two monomers approach. While only 1.3 kcal/mol for SF_4, it grows with enlarging chalcogen atom, to 5.6 and 6.2 kcal/mol for SeF_4 and TeF_4, respectively. In other words, the deformation energy increases as the chalcogen bond gets stronger.

One might think that the MEP on the van der Waals surface of the monomer, approximated by a density of 0.001 au, is a poor indicator of the incipient bonding that occurs at much closer interatomic distance. Another choice would be the density at the bond critical point, which occurs roughly halfway between the bonding atoms. $V_{s,max}$ was thus recomputed for each monomer, on the isodensity surface corresponding to ρ_{BCP} of each complex listed in Table 1. Lying much closer to the nuclei, these maxima displayed in the final column of

Table 1 are of course much more positive [60]. Nonetheless, they share many of the same trends as the 0.001 au maxima in the preceding column. The largest values are associated with the pnicogen bonds, and the smallest with the YF_6 chalcogen bonds. On the other hand, the maxima evaluated at the bond critical points do not necessarily increase with the size of the central atom, as witness the halogen and pnicogen atoms.

Decomposition of the total interaction energy into its various components can offer additional insight into the nature of the bonding. SAPT decomposition of three sample complexes are compiled in Table 2. As the strength of the complex grows in the order halogen < chalcogen < pnicogen bond, so do their various components. ES is the dominant attractive term, followed by induction, and then by dispersion, except for $BrF_5\cdots NH_3$ where the two latter components are nearly equal. The concept of decomposition is a questionable one, however, when the two subunits are close to one another. The $AsF_5\cdots NH_3$ dimer, with a R(As··N) distance of only 2.1 Å, is a prime example. The exaggerated electrostatic and induction components, on the order of 100 kcal/mol, serves as a caution, as does the total SAPT interaction energy of -95 kcal/mol, twice that computed by the standard supermolecule approach.

Of all the interactions considered here, the pnicogen bonds to the pentavalent ZF_5 molecules are the strongest. The binding energy of $SbF_5\cdots NH_3$ reaches up to nearly 40 kcal/mol. The intermolecular distances reflect this bond strength, between 1.9 and 2.2 Å. The strengths of these bonds are reflected also in the AIM values of ρ_{BCP} which exceed 0.1 au in several cases, matched only by the halogen bond in $ClF_5\cdots NH_3$. The binding energy rises quickly along with the size of the pnicogen atom, as does the intensity of the σ-hole. On the other hand, the trends in some of the other quantities do not reflect these trends. For example, ρ_{BCP} is smallest for Z=Sb as is E(2). It might also be noted that the auxiliary E(2)* quantities for the four other Z-F antibonds are quite large for these pnicogen bonds, eclipsing the primary E(2). Another important issue for the ZF_5 systems is the magnitude of the monomer rearrangement upon complexation. Without any lone pair, the monomer adopts a pure trigonal bipyramid shape. As may be seen in Fig 1, in order to accommodate the NH_3, the monomer rearranges into a square pyramid shape. In the case of SbF_5, for example, this rearrangement costs 9.47 kcal/mol. This deformation energy is even larger for the smaller pnicogens, 16.3 and 22.7 kcal/mol for the Br and Cl analogues, respectively. Addition of these deformation energies to the binding energies in Table 1 yields a pure interaction energy, between pre-deformed monomers. These interaction energies are quite large, nearly 50 kcal/mol, and surprisingly insensitive to the nature of the pnicogen atom or to the magnitude of its σ-hole.

3.2 SeF_nH_{6-n}

3.2.1 Relations between MEP maxima and equilibrium geometries

As was shown above, the replacement of several F atoms of TeF_6 by H produces some substantial changes in the complexation process with NH_3. An intensification of the σ-hole occurs, in particular in the H_3 face of

the octahedron. It is this positive region which draws in the base, and thereby forms a strong chalcogen bond. It is of some importance that the base eschews formation of a TeH··N HB in place of this chalcogen bond, nor does one see any NH··F HBs. This result brings to the fore the fundamental issue of how the replacement of highly electronegative atoms by H might affect the ability of the central atom to engage in a chalcogen bond. At what point do YH··N HBs take precedence over such a bond? And might these substitutions induce the formation of one or more NH··F HBs as a replacement for a chalcogen bond.

In order to thoroughly examine this question, the octahedral SeH_6 molecule was taken as a starting point, and then variable numbers of H atoms were replaced by F, all the way up to perfluorinated SeF_6. For each molecule, all maxima on the MEP was identified. Then NH_3 was added and the potential energy surface of the ensuing heterodimer was searched for all energy minima. The types of noncovalent interaction that hold together each dimer were characterized and quantified, and the geometries of the minima related to the location and intensities of MEP maxima.

As F atoms replace H one by one, on the SeH_6 molecule, there can be a number of different conformers. The two F atoms on SeF_2H_4 can be placed either anti or cis to one another, respectively disposed roughly 180° or 90° to one another within the octahedral geometry of the molecule. The three F atoms in SeF_3H_3 can all be within 90° of one another, denoted cis,cis, or one pair can be anti, with the third F cis to both of them, here referred to as anti,cis. When there are more F than H atoms, it becomes more convenient for the notation to refer to the latter, wherein the two H atoms in the cis,cis conformation of SeF_4H_2 can either be anti or cis to one another.

Due to the octahedral structure of SeF_nH_{6-n}, the position directly opposite any particular substituent is occupied by another, precluding the possibility of strict σ-holes opposite any given Se-X/H bond. Most of the locations of $V_{s,max}$ then occur on one of the octahedral faces, denoted by the three atoms on that face. For example, the FH_2 face of $SeFH_5$ is situated between these three atoms, and there are four such faces, all equivalent to one another. There are also four equivalent H_3 faces on this same molecule. In some cases, there is a maximum in the MEP that occurs not on a face of three substituents, but rather between just two substituents. For example, the anti SeF_2H_4 molecule has four equivalent $V_{s,max}$ points in the equatorial SeH_4 plane, each located between a pair of H atoms, so are designated as H_2. Finally, in some cases, there is a maximum along an extension of a Se-F or Se-H covalent bond, i.e. on a vertex of the octahedron, denoted respectively as F or H.

The locations of each maximum are reported in Table 3, including both the value of $V_{s,max}$ and its distance from the central Se where appropriate. The last two columns are related to the equilibrium geometry of the $SeF_nH_{6-n}···NH_3$ dimer that correlates with the particular maximum, wherever such correlations can be drawn. These dimers are illustrated in Fig 2. The first row of Table 3 shows for example, that there is only one

minimum on the surface of $SeF_0H_6\cdots NH_3$, wherein the base lies along the H_3 face of the acid, as depicted in Fig 2a. The equilibrium $R(Se\cdot\cdot N)$ separation is 3.387 Å, and the binding energy of this complex is 0.93 kcal/mol. Replacement of one H atom of SeH_6 by F leads to two types of maxima on the MEP. There is one on each of the four H_3 faces and a single maximum along the extension of the SeH_a bond where the a subscript designates a position axial to the single F atom. The value of $V_{s,max}$ for the former is 29.45 kcal/mol, a bit higher than the 22.83 kcal/mol for the latter. One equilibrium structure (Fig 2c) conforms nicely to the H_3 maximum, bound by 3.63 kcal/mol. The second MEP maximum also relates to an equilibrium structure, in this case bound by a $SeH\cdot\cdot N$ HB. This geometry is bound by less than the former, 2.48 vs 3.63 kcal/mol. But it is instructive to note that the most strongly bound dimer of all does not relate to a maximum in the MEP. This structure, shown in Fig 2b, is bound primarily by a $NH\cdot\cdot F$ HB, with smaller supplements from a pair of $SeH\cdot\cdot N$ HBs (see below for more detailed analysis). The geometry of this structure places the N atom on a FH_2 face but as Table 3 makes clear, there is no MEP maximum on this face.

The anti configuration of SeF_2H_4 contains a single type of MEP maximum between each pair of H atoms in the equatorial plane. That maximum corresponds to the single equilibrium dimer with NH_3, although a $NH\cdot\cdot F$ attraction pulls the NH_3 out of the HSeH plane, toward a FH_2 face, as displayed in Fig 2d. The cis geometry of SeF_2H_4 is also characterized by a single MEP maximum, which occurs in the H_3 face (Fig 2e). Although $V_{s,max}$ for this conformation is quite a bit larger than that for the cis geometry, the binding energy of 5.45 kcal/mol is only slightly larger than 4.37 kcal/mol for the anti configuration. Equilibrium structures were also sought for the FH_2 and F_2H faces of cis SeF_2H_4, but none were found, consistent with the absence of MEP maxima on those faces.

SeF_3H_3 can appear as either anti,cis or cis,cis combinations of the three F atoms. The former arrangement yields only a single MEP maximum on the HSeH bisector. But rather than appear as an equilibrium $SeF_3H_3\cdot\cdot NH_3$ dimer, placement of the base along this position results in a proton transfer to an $SeF_3H_2^-\cdot\cdot NH_4^+$ ion pair. The cis,cis structure displays two separate types of MEP maximum. The first lies in the H_3 face, and is quite positive, with $V_{s,max} = 64.43$ kcal/mol. The binding energy of the associated dimer in Fig 2f is correspondingly large: at -7.25 kcal/mol it represents the most tightly bound dimer of all those considered here. There is a second maximum in the F_3 face, but its $V_{s,max}$ is quite negative, so it is no surprise to see no corresponding equilibrium geometry. On the other hand, there are two equilibrium heterodimers for cis,cis SeF_3H_3 that are unconnected to any MEP maximum. The NH_3 approaches the F_2H and FH_2 faces in these two geometries (Figs 2g and 2h) which are both bound by nearly 6 kcal/mol.

With respect to SeF_4H_2, the anti arrangement of the two H atoms yields a MEP maximum only on the extension of the two SiH bonds. Placement of the NH_3 in this position results in a transfer of the proximate proton directly to the NH_3, yielding the ion pair. When the two H atoms are cis to one another, a MEP

maximum appears between them. Its high $V_{s,max}$ again results in a strongly bound dimer (Fig 2i) of 7.02 kcal/mol. The other maximum, on the F_3 face, is negative so unsurprisingly does not yield a stable dimer of the desired type, but instead rearranges to have a H atom of the NH_3 face the F atoms, engaging in a pair of NH··F HBs, as illustrated in Fig 2j.

There are three MEP maxima when only a single H atom is left on SeF_5H. The most intense occurs along the SeH axis, and another on each F_3 face. But placement of a NH_3 in either position results in a proton transfer to an ion pair. When NH_3 is placed coincident with a F_2H face, no minimum can be located. The eight equivalent MEP maxima on SeF_6 on each F_3 face are fairly positive in sign, with $V_{s,max}$=24.38 kcal/mol, but the ensuing dimer in fig 2k is bound by less than 1 kcal/mol. The weak maxima found along the SeF axes of both SeF_5H and SeF_6 do not yield minima either.

3.2.2 Analysis of Attractive Forces

A cursory inspection of the dimer geometries in Fig 2 leads to questions as to the precise nature of the bonding in each. The roughly C_{3v} structure of the SeF_6··NH_3 complex in Fig 2a, for example, could lead one to surmise the presence of a Se··N chalcogen bond, or one or more SeH··N HBs, or some combination thereof. The same could be said of many of the other equilibrium geometries in Fig 2. As the geometries of these dimers do not immediately and unambiguously point to a single type of attractive force in each, it becomes important to analyze the source of binding. As in the former cases, both AIM and NBO are used for this purpose. In the case of a Se chalcogen bond, it is typical to observe NBO charge transfer from the nonbonding lone pair of the Lewis base to a σ^*(Se-R) antibonding orbital of the Lewis acid, where R is situated directly opposite the approaching base. Due to the octahedral structure of the SeF_nH_{6-n} molecules considered here, the NH_3 cannot lie directly opposite any one Se-R bond so this transfer will generally involve three such bonds, those that are most nearly opposite the N.

The pertinent NBO and AIM parameters are contained in Fig 2. Blue lines are drawn between atoms that are connected by an AIM bond path, along with the interatomic distance in Å (in black). The value of the density at each bond critical point (x10^4 au) is displayed alongside this path, in blue. The red number refers to the NBO value of E(2) (x100 kcal/mol) wherever there is charge transfer from the N lone pair to the appropriate σ^* antibonding orbital. The large black number represents the binding energy of each dimer, and the green number refers to the value of $V_{s,max}$ on the Lewis acid which the NH_3 is approaching, when such a maximum is present.

Taking SF_6··NH_3 in Fig 2a as an example, there are AIM bond paths from the N to two of the H atoms on SF_6, indicating a pair of SeH··N HBs. ρ_{BCP} is equal to 0.0085 au for each of these bonds, and there is a small $N_{lp} \rightarrow \sigma^*$(Se-H) charge transfer energy of 0.09 kcal/mol for each. (The latter two values are only displayed for one of these two equivalent bonds to avoid needless clutter of the figure.) There is discrepancy between the two

methods with respect to a possible Se··N chalcogen bond. Whereas there is no AIM bond path between these two atoms, NBO indicates 0.27 kcal/mol of charge transfer from the N lone pair to the antibonding orbitals of the three Se-H bonds that are turned away from the N. Note that altogether these three interactions account for a total binding energy of less than 1 kcal/mol, consistent with their weakness, as well as the small value of $V_{s,max}$ of only 12.3 kcal/mol.

Neither AIM nor NBO suggest a chalcogen bond in Fig 1b where the two molecules are held together primarily by a NH··F HB which, with ρ_{BCP}=0.0153 au and E(2)=4.01 kcal/mol, is a rather strong one. This interaction is supplemented by a pair of reasonably strong SeH··N HBs, for a total binding energy of 4.06 kcal/mol. Neither AIM nor NBO suggest the presence of a chalcogen bond, which is not surprising in light of both the orientation of the NH_3 lone pair away from the Se, and the absence of a MEP maximum on the FH_2 face of the $SeFH_5$ molecule. The H_3 face of this same molecule contains a MEP maximum of magnitude 29 kcal/mol, so the geometry of the complex in Fig 1c turns the NH_3 lone pair more in line with the Se atom. Nonetheless, the Se··N chalcogen bond remains weak, with E(2) equal to only 0.44 kcal/mol, and no AIM bond path. Like the other geometry of this dimer, there are a pair of SeH··N HBs that help stabilize it. It should be noted that the SFH_5 molecule also shows a MEP maximum along the Se-H axis (directly opposite Se-F), which leads to a geometry with a linear SeH··N HB and no hint of a chalcogen bond. However, this structure is not quite as stable as the two illustrated in Fig 2.

The anti SeF_2H_4 complex with NH_3 in Fig 2d contains three HBs, all of moderate strength, supplemented by what appears to be only a weak chalcogen bond. The cis configuration of this same acid, however, is characterized by a fairly intense σ-hole of 48.3 kcal/mol on its H_3 face which induces the NH_3 to turn its lone pair toward the Se, forming a Se··N chalcogen bond, measured by NBO E(2)=0.99 kcal/mol, as indicated in Fig 2e. Note that this value of E(2) exceeds the 0.79 kcal/mol for the SeH··N HB, but it is only the latter that is characterized by an AIM bond path.

Turning next to trisubstituted SeF_3H_3 the anti,cis conformer has a MEP maximum between each pair of H atoms, which is fairly intense at 48.7 kcal/mol. However, there is no equilibrium geometry of the dimer that corresponds to this position. The cis,cis conformer is interesting for a number of reasons. The three F atoms on cis-SeF_3H_3 intensify the σ-hole on its H_3 face to 64 kcal/mol, leading to what is probably the strongest chalcogen bond of those examined here, with R(Se··N)=3.11 Å and E(2)=2.25 kcal/mol. It is in this structure in Fig 2f that AIM for the first time confirms the presence of a chalcogen bond, with ρ_{BCP}=0.0118 au. With some supplementation by three SeH··N HBs, the total binding energy rises to 7.25 kcal/mol. (Note, however, that the latter HBs are manifested only in AIM, with no evidence of the NBO charge transfer that is characteristic of such bonds.) The other two structures involve the F_2H and FH_2 faces of SeF_3H_3 in Figs 2g and 2h, but it is worth emphasizing that neither of these faces contains a MEP maximum. Both of these complexes depend

almost exclusively on HBs, with only weak indications of a chalcogen bond. And both are bound less tightly than is the chalcogen-bonded structure in Fig 2f. There is a maximum on the F_3 face of this molecule, but $V_{s,max}$ is quite negative so it is not surprising that there is no equilibrium geometry to which it corresponds.

The anti geometry of SeF_4H_2 contains a MEP maximum only along each SeH bond and does not lead to a minimum on the potential energy surface. The large value of $V_{s,max}$ on the HSeH bisector of the cis monomer better orients the NH_3 lone pair in Fig 2i, and E(2) for the chalcogen bond exceeds 1 kcal/mol. After supplementation by a pair of moderately strong SeH··N HBs, the binding energy reaches 7.02 kcal/mol. Considering the MEP maximum on the F_3 face, its negative value leads to a rearrangement to the bifurcated HB configuration in Fig 2j, bound by only 1.14 kcal/mol. As indicated in Table 3, the only $V_{s,max}$ of any consequence for SeF_5H occurs along the Se-H bond extension, so no stable dimer of the sort that might contain a chalcogen bond is present. The perfluorinated SeF_6 displays a MEP maximum on each of its F_3 faces which attracts the NH_3 molecule to this area. The complex does not contain a chalcogen bond, but instead relies for its weak attraction on a pair of distorted NH··F HBs. Note in Fig 2k that these bonds are so weak that there is little indication of their presence via NBO analysis.

4. DISCUSSION

In summary, the pentavalent ZF_5 molecules engage in the strongest interactions with NH_3. These pnicogen bond energies range between 25 and 37 kcal/mol, despite their burden of a substantial monomer deformation energy as ZF_5 converts from a trigonal bipyramid to a square pyramid shape. When these distortions are factored in, the interaction energies between pre-deformed monomers are even larger, ranging up to 48 kcal/mol, and might even be characterized as partial covalent bonds. The chalcogen bonds involving tetravalent central atoms are not as strong but not weak by any means, covering the 6.6 - 16.0 kcal/mol range. Like the pnicogen bonds, these chalcogen bonds also strengthen as the central atom is enlarged. Halogen bonds involving XF_5 show an unusual pattern in that it is the lightest X=Cl atom which displays the strongest bond, with both Br and I roughly half that magnitude. By far the weakest of all are the interactions between hexavalent YF_6 and NH_3. In fact, these interactions would probably not even be categorized as chalcogen bonds at all, but are bound primarily by weak NH··F H-bonds. The presence of a lone pair on the central atom affects the position and magnitude of σ-holes, and influences angular characteristics of the complexes to a varying degree.

While the intensity and location of maxima on the MEP offer some guidance as to geometries and strengths of noncovalent bonds, they represent a clearly imperfect marker. On one hand, $V_{s,max}$ increases as the central atom grows in size for any central atom type, as does the binding energy. But in terms of comparison of the various bond types, there are some misleading patterns. For example, even though the YF_4 σ-holes are comparable to those for ZF_5, the binding and interaction energies of the former with NH_3 are very much smaller

than those of the latter. The steric crowding in the octahedral YF_6 molecules prevent formation of significant chalcogen bonds, even when $V_{s,max}$ achieves a respectable magnitude as in TeF_6. But this problem can be countered to some extent by replacing three of the F atoms by H, which reduces steric repulsion and doubles the value of $V_{s,max}$.

The additional substituents connected with hypervalency do more than simply crowd the central atom and potentially obstruct the path of a base toward it. The molecular geometries place σ-bonds directly opposite one another, which block the development of σ-holes. Lone pairs adopt positions that can either conflict directly with a σ-hole, displace it from its normally preferred direction, or weaken its intensity. Each of the hypervalent systems displays unique properties in this regard. In the case of halogen bonds, the base is able to approach the central halogen atom of XF_5 opposite the apical F atom of the square pyramidal molecule to engage in a reasonably strong halogen bond. This direction presents a conflict in that the X lone pair would produce a negative MEP, while a positive potential is associated with the XF antibonding orbital. As a result the MEP maxima are shifted away from the linear direction by 33°, 37°, and 45° respectively for Cl, Br, and I. The competition between these two effects is dependent upon the nature of the X atom. The $θ(FX··N)$ angle varies from 180° for Cl, to 168° for Br, and 145° for I. In other words, the base is drawn closer toward the linear FX··N direction than would be the case if it were fully controlled by the $V_{s,max}$ position. There is little need for the spacious square pyramid to alter its shape to accommodate the base so the XB forms with very little deformation energy.

The Y lone pair in YF_4 lies in the equatorial plane, but not directly opposite any of the F-S bonds, so consequently only nudges the $V_{s,max}$ 12-15° from lying directly opposite these bonds. This deviation is reflected in the nonlinearity of the $YF_4··NH_3$ dimers, which again grows stronger along with the size of the central atom. As in the previous case, not much rearrangement is required to accommodate the base, so the deformation energies are modest. The ZF_5 molecules undergo the most severe deformation, shifting their structure from trigonal bipyramid to square planar. Z has no lone pairs, so the base is free to approach directly opposite the apical F atom, with $θ(FZ··N)=180°$. Since the intermolecular steric interactions are small, the deformation energy arises from the internal rearrangement. It is in the YF_6 cases where intermolecular steric crowding is dominant. The fairly rigid octahedral shape prevents the F atoms from getting out of the way of the approaching base, which keeps the intermolecular distance long and the binding energies minimal, despite reasonably large values of $V_{s,max}$.

In connection with the interchange of F and H substituents, there are clear patterns seen when the H atoms of SeH_6 are replaced one by one by the much more electronegative F. The NH_3 is generally able to approach within bonding distance of the Lewis acid, despite the latter's crowded octahedral structure. The bonding is quite weak for SeH_6 but builds quickly as the H atoms are progressively replaced by F. The peak occurs when

the NH_3 approaches the H_3 face of SeF_3H_3 where the N lone pair can transfer charge into three $\sigma^*(Se-F)$ antibonding orbitals in an unambiguous chalcogen bond. The strength of this interaction is aided by a rather intense MEP maximum that also lies on the H_3 face. Due to the congested nature of these acids, there are few dimer geometries which contain only a single type of attractive interaction. The aforementioned SeF_3H_3 complex, for example, also contains elements of three weaker $SeH\cdot\cdot N$ HBs. On that same line, the strongest interactions generally involve the approach of the NH_3 toward the H atoms of the Lewis acid, whether that involves $SeH\cdot\cdot N$ HBs or a bona fide $Se\cdot\cdot N$ chalcogen bond. It is this region which generally provides the most positive MEP, although a number of stable dimers occur where there is no MEP maximum at all. These cases tend to invoke one or more $NH\cdot\cdot F$ HBs as the N lone pair turns away from the electronegative F atoms, leaving the NH_3 protons to better approach the latter.

Not all MEP maxima lead to equilibrium geometries, nor is such a maximum necessary for such a structure to arise. In the $SeFH_5$ case for example, its most stable dimer with NH_3 is not connected to a maximum in the MEP. The same can be said of the cis,cis conformer of SeF_3H_3, where two of the three optimized dimers, with binding energies in excess of 5 kcal/mol, do not have a corresponding $V_{s,max}$. Conversely, the anti,cis conformation of this same SeF_3H_3 displays a single MEP maximum, but no associated equilibrium structure. In some cases, the optimization beginning with the appropriate chalcogen bond led instead to $SeH\cdot\cdot N$ or $NH\cdot\cdot F$ HBs, or some combination thereof. This lack of a strict correlation between $V_{s,max}$ and equilibrium structure is consistent with some prior calculations. In the halogen bonds formed by CX_3I, for example, $V_{s,max}$ was observed [61, 62] to be a poor indicator of the interaction energy, and may not even correlate well with the full electrostatic component.

There are other studies in the literature that offer a means of testing the validity of the calculations presented here. Most of the prior work dealing with noncovalent interactions of hypervalent atoms concerns halogen bonds. A search of diffraction data in the Cambridge Structure Database (CSD) found [23] more than 70 crystal structures where hypervalent halogen acts as a Lewis acid. Theoretical calculations suggested that halogen bond strengths involving trivalent X were roughly equivalent to their monovalent analogues. Like our own study of XF_5, these authors also noted secondary NBO charge transfer to the antibonding orbitals that are peripheral to the $X\cdot\cdot N$ axis. Grabowski later expanded to both trivalent and pentavalent halogens [24, 25] and found that the σ-holes on pentavalent halogen atoms are somewhat weaker than their trivalent analogues, as are the halogen bond strengths. Some deviations from linearity occurred in the pentavalent cases as well due in part to the presence of lone electron pairs, confirming our own optimized geometries. He noted charge transfers to peripheral covalent bonds, in line with the earlier findings [23]. Hypervalent FXO_n molecules were considered, with n as large as 3, in terms of their ability to form XBs [63] but these bonds were contaminated with HBs as well for n>1. Nonetheless, there did not appear to be much sensitivity to the binding energy as O atoms were

added to the central X. Kirshenboim and Kozuch [27] delved into the mechanisms whereby the σ-holes surrounding tri and pentavalent halogens atoms are affected by the peripheral substituents and the halogen lone pair, which can force the holes to misalign with the covalent bonds, confirming our own data above. More recent calculations [26] suggest a steady erosion of the halogen bond strength on going from mono to tri to pentavalent bonding. As in our own calculations, the base deviates significantly from a position directly opposite the apical F atom of BrF_5.

Although still meager, there are a few studies of hypervalent pnicogen bonds. Extension of the valency of pnicogens to tetravalency [31] in ZOF_2X and ZOF_3 showed stronger binding of Z=As as compared to P, consistent with our findings here of the pentavalent analogues. The bond critical point densities of the complexes with NH_3 were only slightly less than our own data for the pentavalent pnicogen bonds. Unfortunately the authors did not specify geometrical changes in the monomer to accommodate the base, nor the energetic consequence of any such distortion. Crystal studies [33] confirm our rearrangement whereby a pentavalent ZF_5 molecule normally in a trigonal bipyramid shape molds itself into a square pyramidal arrangement upon formation of a pnicogen bond. Pentavalent pnicogen bonds to pyrazines were very recently examined by Fanfrlik et al [64] from both a theoretical and experimental perspective. The authors found monomer rearrangements similar to those described here, with comparable deformation energies, which were directly linked to a strengthening of the relevant σ-holes. Previous calculations [28] of the S··N chalcogen bond involving SF_4 and a series of N-bases found chalcogen bond energies comparable to that in Table 1. Also confirmed there was the NBO charge transfer into peripheral S-F antibonding orbitals. There was little change when SF_4 was changed to a simple divalent SF_2. The geometries of these complexes are verified by earlier diffraction and spectroscopic measurements [65]. The very weak bonding of SF_6 with NH_3, as well as its geometry, is consistent with an earlier microwave study of this complex [66]

In conclusion, hypervalency presents the study of noncovalent interactions with additional complexity. Issues related to steric repulsion, monomer deformation and rearrangement, displacement of MEP maxima by lone pairs, or complete absence thereof due to opposite placement of σ-bonds, must all be considered. Depending on the particular combination of these factors, the noncovalent bond may be eliminated, whereas this bond can be strengthened in others.

REFERENCES

[1]   G. Gilli, P. Gilli, The Nature of the Hydrogen Bond, Oxford University Press, Oxford, UK, **2009**.
[2]   G. R. Desiraju, T. Steiner, The Weak Hydrogen Bond in Structural Chemistry and Biology, Oxford, New York, **1999**.
[3]   S. Scheiner, Hydrogen Bonding. A Theoretical Perspective, Oxford University Press, New York, **1997**.
[4]   S. J. Grabowski in Hydrogen Bonding - New Insights, Vol. (Ed.^Eds.: Editor), Springer, City, **2006**.
[5]   I. Alkorta, S. Rozas, J. Elguero *J. Phys. Chem. A.* **1998**, *102*, 9278-9285.
[6]   A. Karpfen *J. Phys. Chem. A.* **2000**, *104*, 6871-6879.
[7]   W. Zierkiewicz, R. Wieczorek, P. Hobza, D. Michalska *Phys. Chem. Chem. Phys.* **2011**, *13*, 5105-5113.
[8]   K. E. Riley, C. L. Ford Jr, K. Demouchet *Chem. Phys. Lett.* **2015**, *621*, 165-170.
[9]   P. Politzer, J. S. Murray in *A unified view of halogen bonding, hydrogen bonding and other σ-hole interactions, Vol. 19* (Ed. S. Scheiner), Springer, Dordrecht, Netherlands, **2015**, pp.357-389.
[10] S. Scheiner *Chem. Phys.* **2011**, *387*, 79-84.
[11] W. Zierkiewicz, D. C. Bieńko, D. Michalska, T. Zeegers-Huyskens *J. Comput. Chem.* **2015**, *36*, 821-832.
[12] U. Adhikari, S. Scheiner *J. Phys. Chem. A.* **2014**, *118*, 3183-3192.
[13] A. Bauzá, T. J. Mooibroek, A. Frontera *Angew. Chem. Int. Ed.* **2013**, *52*, 12317-12321.
[14] J. E. Del Bene, I. Alkorta, J. Elguero in *The pnicogen bond in review: Structures, energies, bonding properties, and spin-spin coupling constants of complexes stabilized by pnicogen bonds, Vol. 19* (Ed. S. Scheiner), Springer, Dordrecht, Netherlands, **2015**, pp.191-263.
[15] Z. Latajka, S. Scheiner *J. Chem. Phys.* **1987**, *87*, 1194-1204.
[16] G. Sanchez-Sanz, C. Trujillo, I. Alkorta, J. Elguero *Phys. Chem. Chem. Phys.* **2016**, *18*, 9148-9160.
[17] S. J. Grabowski *Phys. Chem. Chem. Phys.* **2014**, *16*, 1824-1834.
[18] I. Alkorta, I. Rozas, J. Elguero *J. Phys. Chem. A.* **2001**, *105*, 743-749.
[19] S. Scheiner *CrystEngComm.* **2013**, *15*, 3119-3124.
[20] M. Marín-Luna, I. Alkorta, J. Elguero *Theor. Chem. Acc.* **2017**, *136*, 41-.
[21] M. Liu, Q. Li, S. Scheiner *Phys. Chem. Chem. Phys.* **2017**, *19*, 5550-5559.
[22] T. Clark, M. Hennemann, J. S. Murray, P. Politzer *J. Mol. Model.* **2007**, *13*, 291-296.
[23] W. Wang *J. Phys. Chem. A.* **2011**, *115*, 9294-9299.
[24] S. J. Grabowski *Chem. Phys. Lett.* **2014**, *605-606*, 131-136.
[25] S. J. Grabowski *Phys. Chem. Chem. Phys.* **2017**, *19*, 29742-29759.
[26] G. J. Buralli, D. J. R. Duarte, G. L. Sosa, N. M. Peruchena *Struct. Chem.* **2017**, *28*, 1823-1830.
[27] O. Kirshenboim, S. Kozuch *J. Phys. Chem. A.* **2016**, *120*, 9431-9445.
[28] V. d. P. N. Nziko, S. Scheiner *J. Phys. Chem. A.* **2014**, *118*, 10849-10856.
[29] M. D. Esrafili, F. Mohammadian-Sabet *Struct. Chem.* **2016**, *27*, 617-625.
[30] M. D. Esrafili, R. Nurazar *Mol. Phys.* **2016**, *114*, 276-282.
[31] M. D. Esrafili, N. Mohammadirad *Struct. Chem.* **2016**, *27*, 939-946.
[32] B. Khalili, M. Rimaz *Struct. Chem.* **2017**, *28*, 1065-1079.
[33] P. Scilabra, G. Terraneo, G. Resnati *J. Fluor. Chem.* **2017**, *203*, 62-74.
[34] M. D. Esrafili, E. Vessally *Chem. Phys. Lett.* **2016**, *662*, 80-85.
[35] M. Gawrilow, H. Beckers, S. Riedel, L. Cheng *J. Phys. Chem. A.* **2018**, *122*, 119-129.
[36] A. Bauza, A. Frontera *Phys. Chem. Chem. Phys.* **2015**, *17*, 24748-24753.
[37] A. Bauzá, A. Frontera *ChemPhysChem.* **2015**, *16*, 3625-3630.
[38] M. J. Frisch, G. W. Trucks, H. B. Schlegel, G. E. Scuseria, M. A. Robb, J. R. Cheeseman, G. Scalmani, V. Barone, B. Mennucci, G. A. Petersson, H. Nakatsuji, M. Caricato, X. Li, H. P. Hratchian, A. F. Izmaylov, J. Bloino, G. Zheng, J. L. Sonnenberg, M. Hada, M. Ehara, K. Toyota, R. Fukuda, J. Hasegawa, M. Ishida, T. Nakajima, Y. Honda, O. Kitao, H. Nakai, T. Vreven, J. Montgomery, J. A., J. E. Peralta, F. Ogliaro, M. Bearpark, J. J. Heyd, E. Brothers, K. N. Kudin, V. N. Staroverov, R. Kobayashi, J. Normand, K. Raghavachari, A. Rendell, J. C. Burant, S. S. Iyengar, J. Tomasi, M. Cossi, N. Rega, J. M. Millam, M. Klene, J. E. Knox, J. B. Cross, V. Bakken, C. Adamo, J. Jaramillo, R. Gomperts, R. E. Stratmann, O. Yazyev, A. J. Austin, R. Cammi, C. Pomelli, J. W. Ochterski, R. L. Martin, K. Morokuma,

V. G. Zakrzewski, G. A. Voth, P. Salvador, J. J. Dannenberg, S. Dapprich, A. D. Daniels, O. Farkas, J. B. Foresman, J. V. Ortiz, J. Cioslowski, D. J. Fox in Gaussian 09, **2009**.

[39]   D. Feller *J. Comput. Chem.* **1996**, *17*, 1571-1586.

[40]   K. L. Schuchardt, B. T. Didier, T. Elsethagen, L. Sun, V. Gurumoorthi, J. Chase, J. Li, T. L. Windus *J. Chem. Infor. Model.* **2007**, *47*, 1045-1052.

[41]   L. Spada, Q. Gou, Y. Geboes, W. A. Herrebout, S. Melandri, W. Caminati *J. Phys. Chem. A.* **2016**, *120*, 4939-4943.

[42]   R. Shukla, D. Chopra *Phys. Chem. Chem. Phys.* **2016**, *18*, 13820-13829.

[43]   Q. Tang, Q. Li *Comput. Theor. Chem.* **2015**, *1070*, 21-26.

[44]   Y. Geboes, F. D. Proft, W. A. Herrebout *J. Phys. Chem. A.* **2015**, *119*, 5597-5606.

[45]   D. Sutradhar, A. K. Chandra, T. Zeegers-Huyskens *Mol. Phys.* **2014**, *112*, 2791-2801.

[46]   G. Sanchez-Sanz, C. Trujillo, I. Alkorta, J. Elguero *Phys. Chem. Chem. Phys.* **2014**, *16*, 15900-15909.

[47]   M. D. Esrafili, P. Fatehi, M. Solimannejad *Comput. Theor. Chem.* **2014**, *1034*, 1-6.

[48]   D. Hauchecorne, W. A. Herrebout *J. Phys. Chem. A.* **2013**, *117*, 11548-11557.

[49]   X. Liu, J. Cheng, Q. Li, W. Li *Spectrochim. Acta A.* **2013**, *101*, 172-177.

[50]   S. F. Boys, F. Bernardi *Mol. Phys.* **1970**, *19*, 553-566.

[51]   M. Gutowski, F. B. van Duijneveldt, G. Chalasinski, L. Piela *Chem. Phys. Lett.* **1986**, *129*, 325-330.

[52]   T. Lu, F. Chen *J. Comput. Chem.* **2012**, *33*, 580-592.

[53]   E. D. Glendening, C. R. Landis, F. Weinhold *J. Comput. Chem.* **2013**, *34*, 1429-1437.

[54]   R. F. W. Bader, M. T. Carroll, J. R. Cheeseman, C. Chang *J. Am. Chem. Soc.* **1987**, *109*, 7968-7979.

[55]   R. F. W. Bader, Atoms in Molecules, A Quantum Theory, Clarendon Press, Oxford, **1990**.

[56]   T. A. Keith in AIMALL, Vol. (Ed.^Eds.: Editor), TK Gristmill Software, City, **2013**.

[57]   K. Szalewicz, B. Jeziorski in *Symmetry-adapted perturbation theory of intermolecular interactions, Vol.* (Ed. S. Scheiner), Wiley, New York, **1997**, pp.3-43.

[58]   R. Moszynski, P. E. S. Wormer, B. Jeziorski, A. van der Avoird *J. Chem. Phys.* **1995**, *103*, 8058-8074.

[59]   H.-J. Werner, P. J. Knowles, G. Knizia, F. R. Manby, M. Schütz, P. Celani, T. Korona, R. Lindh, A. Mitrushenkov, G. Rauhut, K. R. Shamasundar, T. B. Adler, R. D. Amos, A. Bernhardsson, A. Berning, D. L. Cooper, M. J. O. Deegan, A. J. Dobbyn, F. Eckert, E. Goll, C. Hampel, A. Hesselmann, G. Hetzer, T. Hrenar, G. Jansen, C. Köppl, Y. Liu, A. W. Lloyd, R. A. Mata, A. J. May, S. J. McNicholas, W. Meyer, M. E. Mura, A. Nicklass, D. P. O'Neill, P. Palmieri, K. Pflüger, R. Pitzer, M. Reiher, T. Shiozaki, H. Stoll, A. J. Stone, R. Tarron, T. Thorsteinsson, M. Wang, A. Wolf in MOLPRO, version 2010.1, a package of ab initio programs,

[60]   S. Scheiner *J. Comput. Chem.* **2018**, *39*, 500-510.

[61]   S. M. Huber, E. Jimenez-Izal, J. M. Ugalde, I. Infante *Chem. Commun.* **2012**, *48*, 7708-7710.

[62]   J. Thirman, E. Engelage, S. M. Huber, M. Head-Gordon *Phys. Chem. Chem. Phys.* **2018**, *20*, 905-915.

[63]   N. Cheng, F. Bi, Y. Liu, C. Zhang, C. Liu *New J. Chem.* **2014**, *38*, 1256-1263.

[64]   J. Fanfrlík, W. Zierkiewicz, P. Švec, Z. Růžičková, J. Řezáč, M. Michalczyk, A. Růžička, D. Michalska, P. Hobza *J. Mol. Model.* **2017**, *23*, 328.

[65]   P. Chaudhary, J. T. Goettel, H. P. A. Mercier, S. Sowlati-Hashjin, P. Hazendonk, M. Gerken *Chem. Eur. J.* **2015**, *21*, 6247-6256.

[66]   D. M. Bittner, D. P. Zaleski, S. L. Stephens, N. R. Walker, A. C. Legon *ChemPhysChem.* **2015**, *16*, 2630-2634.

Table 1. Equilibrium geometries, energetics, and other properties of complexes of AF_n with NH_3.

AF_n[a]	R Å	$-E_b$ kcal/mol	$-E_{int}$ kcal/mol	ρ_{BCP} au	E(2) kcal/mol	E(2)*,[b] kcal/mol	$V_{s,max}(\rho=0.001)$ kcal/mol	$V_{s,max}(\rho_{BCP})$ kcal/mol
halogen (1)								
ClF_5	2.067	16.93	46.82	0.1130	217.92	0.99/2	45.1	680.2
BrF_5	2.713	8.56	9.42	0.0310	3.84	5.69/4	53.6	259.2
IF_5	2.912	9.36	9.79	0.0243	2.01	5.54/2	64.2	272.5
chalcogen (0)								
SF_6	3.976	0.25	0.57	0.0039[c]	0	0.28/2[e]	17.0	41.6
SeF_6	3.974	0.62	0.66	0.0041[c]	0	0.33/2[e]	24.4	59.2
TeF_6	3.764	1.04	1.40	0.0064[d]	0.33/3	0	38.1	118.2
TeF_3H_3	3.165	7.57	7.76	0.0126	3.15/3	0.36/3[e]	70.0	176.8
chalcogen (1)								
SF_4	2.573	6.62	7.97	0.0337	14.69	3.71/1	50.7	273.5
SeF_4	2.354	10.99	15.64	0.0579	42.75	12.63/3	60.9	486.5
TeF_4	2.404	16.00	22.23	0.0574	31.66	24.05/3	69.0	552.5
pnicogen (0)								
PF_5	1.915	24.98	47.64	0.1056	38.04	95.32/4	48.0	1377.1
AsF_5	2.014	31.55	47.84	0.1027	33.74	98.43/4	60.5	934.2
SbF_5	2.204	37.46	46.93	0.0785	29.83	86.59/4	82.5	728.1

[a]number of lone pairs on central atom in parentheses
[b]Total charge transfer into peripheral antibonds, with number of such bonds after /
[c]average of $\rho(N{\cdot}{\cdot}F)$ and two $\rho(H{\cdot}{\cdot}F)$
[d]each of 3 $\rho(N{\cdot}{\cdot}F)$
[e]$F_{lp}{\rightarrow}\sigma^*(NH)$

Table 2. SAPT contributions to total interaction energy (kcal/mol) of Lewis acids with NH_3.

AF_n	ES	EX	IND[a]	DISP[b]	total
BrF_5	-22.84	25.87	-4.31	-4.91	-6.19
SeF_4	-53.53	68.20	-23.07	-8.96	-17.37
AsF_5	-117.59	135.15	-99.82	-13.20	-95.47

[a]includes exchange-induction term
[b]includes exchange-dispersion term

Table 3. Locations and values of MEP maxima surrounding SeF_nH_{6-n}, and equilibrium intermolecular separation and binding energy of complexes of each with NH_3.

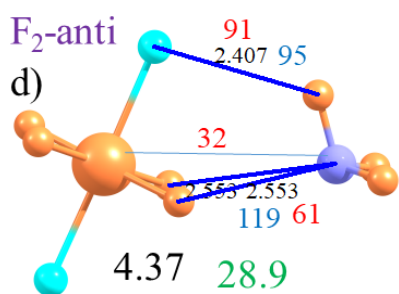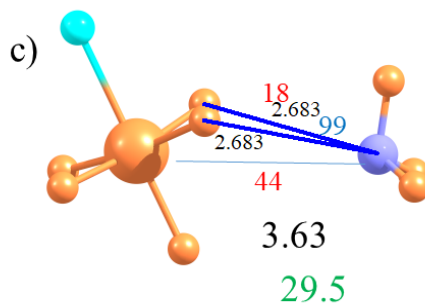| F	H		face	$V_{s,max}$ kcal/mol	R(Se-V) Å	R(Se-N) Å	$-E_b$ kcal/mol	bonding source
0	6		H_3	12.33	2.164	3.387	0.93	2 SeH··N
1	5		FH_2	No max	-	3.350	4.06	2 SeH··N NH··F
			H_3	29.45	2.148	3.332	3.63	2 SeH··N
			H_a	22.83	-		2.48	SeH··N
2	4	anti	H_2	28.90	2.239	3.280	4.37	2 SeH··N NH··F
		cis	H_3	48.29	2.106	3.246	5.45	SeH··N
3	3	anti, cis	H_2	48.68	2.181	no min		3 SeH··N
		cis, cis	H_3	64.43	2.036	3.110	7.25	
			F_2H	No max		3.306	5.74	SeH··N 2 NH··F
			FH_2	No max		3.289	5.63	2 SeH··N NH··F
			F_3	-22.66		no min		
4	2	anti	H	49.35		no min		
		cis	H_2	61.36	2.139	3.174	7.02	2 SeH··N
			F_3	-4.10	2.245	-	1.14	bif NH-F
5	1		F_3	11.37	2.168	no min		
			H	55.93		no min		
			F	-6.79		no min		
6	0		F_3	24.38	1.719	3.976	0.62	2 NH··F N··F
			F	0.58		no min		
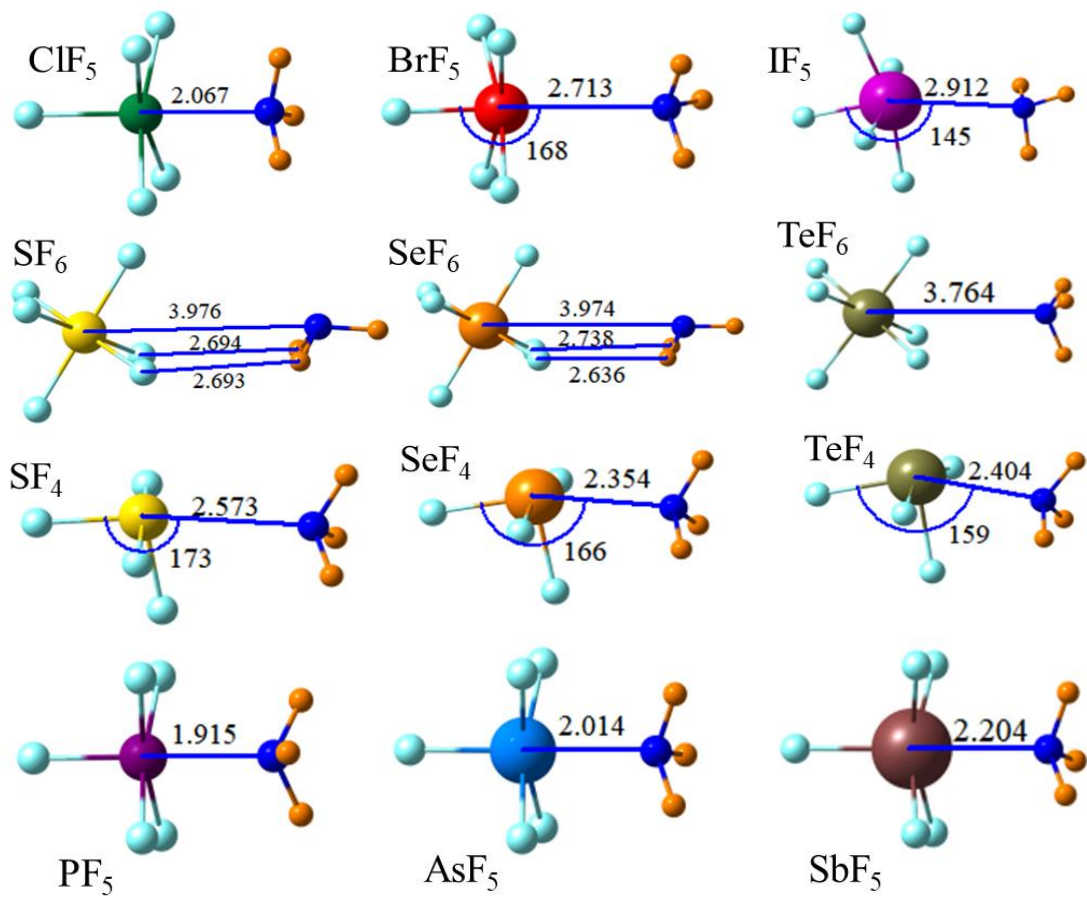
Fig 1. Equilibrium geometries of indicated molecules with NH₃. Distances in Å, angles in degs.

a) F$_0$

85 9
2.789
2.791
27

0.93
12.3

b) F$_1$

401
2.146 153
0
2.612
2.611
40 102

4.06

no max

c)

18
2.683 99
2.683
44

3.63

29.5

d) F$_2$-anti

91
2.407 95
32
2.553 2.553
119 61

4.37   28.9

e) F$_2$-cis

119 79
2.583
99

5.45   48.3

F$_3$-cis,cis

f)

2.673
2.672 119
3.110 118
225
2.673
119

7.25   64.4

g)

249 1119
2.085
12
2.623
65 2.633 23

5.74   no max

h)

2.414 94
106 38
2.620
52
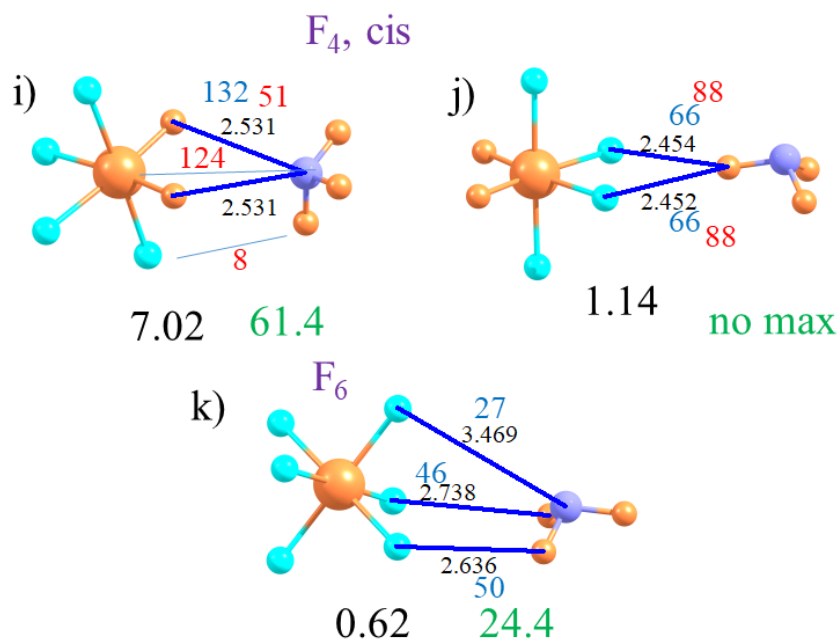2.618
106 38

5.63   no max

22
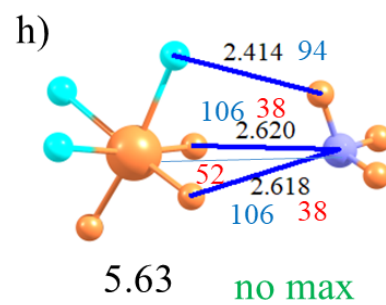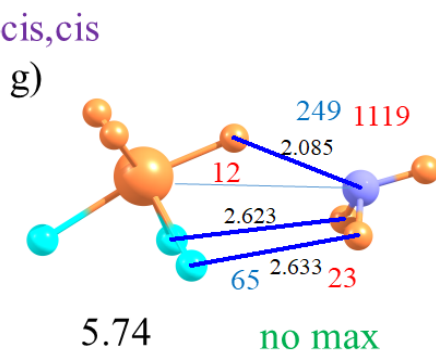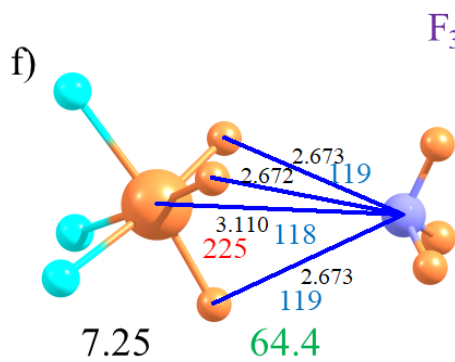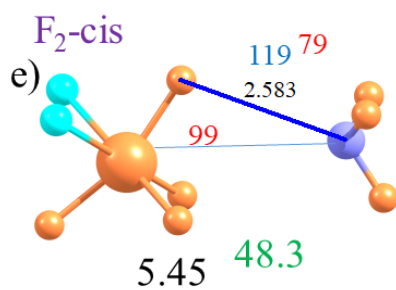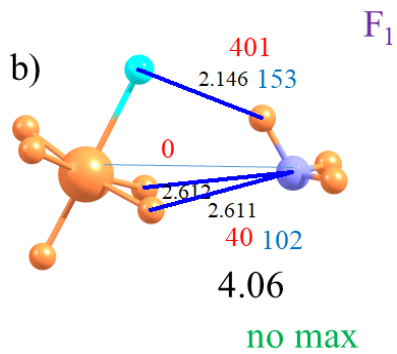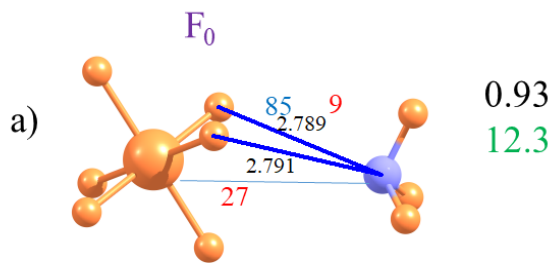
Fig 2. Equilibrium geometries of complexes of NH_3 with SeF_nH_{6-n}. Distance in Å as black numbers shown for interactions marked by an AIM bond critical point, with ρ_{BCP} in blue (10^4 au). NBO values of E(2) (10^2 kcal/mol) shown in red. Large black number refers to binding energy (kcal/mol), and large green number to the value of $V_{s,max}$ (kcal/mol) at the site nearest the N position (if such a maximum exists in that region).

trigonal bipyramid

square pyramid

rearrangement

pentavalent
pnicogen bond
37.5 kcal